Article ID: 1000-7032(2023)08-1380-10

Adjusting Emission Behaviors of Molecules Based Benzothiadiazole by Intermolecular Interaction and Mechano-responsive

DONG Shufan[1], YANG Tingting[2], WEN Zhengjie[1], WANG Yating[1], XU Huixia[1*], DONG Wenjian[1], ZHAO Song[1], WANG Hua[1]

(1. *Key Laboratory of Interface Science and Engineering in Advanced Materials, Ministry of Education, Taiyuan University of Technology, Taiyuan* 030024, *China*;
2. *Shanxi Province Key Laboratory of Microstructure Functional Materials Institute of Solid-state Physical, School of Physics and Electronic Science, Shanxi Datong University, Datong* 037009, *China*)
* *Corresponding Author, E-mail: xuhuixia@tyut. edu. cn*

Abstract: It is a feasible way to adjust emission behaviors by molecular conformation and intermolecular interactions. Herein, two multifunctional materials, 4,4′-(benzo[c][1,2,5]thiadiazole-4,7-diyl)bis(N,N-diphenylaniline) and 4-(7-(9,9-dimethylacridin-10(9H)-yl)benzo[c][1,2,5]thiadiazol-4-yl)-N,N-diphenylaniline, namely **TBT** and **DBT**, with donor-acceptor-donor (D-A-D) and D-A-D′ structures composed of 2,1,3-benzothiadiazole (BT) acceptor and the different donors of triphenylamine (TPA) and 9,9-dimethyl-9,10-dihydroacridine (DMAC) were synthesized. These materials exhibit not only polymorphism-dependent emission but also multicolor luminescence switch in response to the external stimulus. The high-contrast crystal-dependent emission behaviors of **TBT** (**TBT-O**: λ_{PL}=593 nm and **TBT-R**: λ_{PL}=616 nm) and **DBT**(**DBT-Y**: λ_{PL}=570 nm, **DBT-O**: λ_{PL}=605 nm and **DBT-R**: λ_{PL}=642 nm) were observed. **TBT** with double TPA groups exhibits four reversible color switches, while **DBT** with TPA and DMAC groups shows irreversible bicolor change.

Key words: benzothiadiazole; mechanochromic responses; multicolor luminescence
CLC number: O482.31 **Document code**: A **DOI**: 10.37188/CJL.20230022

通过分子间相互作用和机械响应调节苯并噻二唑基分子的发光行为

董书凡[1], 杨婷婷[2], 文峥杰[1], 王雅婷[1], 许慧侠[1*], 董文健[1], 赵 松[1], 王 华[1]

(1. 太原理工大学 新材料界面科学与工程教育部重点实验室, 山西 太原 030024;
2. 山西大同大学 微结构功能材料固体物理研究所山西省重点实验室, 山西 大同 037009)

摘要: 通过分子构型和分子间相互作用是调节材料的发光颜色和光物理性能的重要途径之一。本文以苯并噻二唑为受体(A)、三苯胺(TPA)和二甲基吖啶(DMAC)为给体(D),设计并合成了两种D-A-D和D-A-D′型的发光分子,分别为**TBT** 和 **DBT**。两种分子均表现出同质多晶现象(**TBT-O**: λ_{PL}=593 nm 和 **TBT-R**: λ_{PL}=616 nm; **DBT-Y**: λ_{PL}=570 nm, **DBT-O**: λ_{PL}=605 nm 和 **DBT-R**: λ_{PL}=642 nm)。在外界刺激下,对称结构的**TBT**为四色

收稿日期: 2023-02-03; **修订日期**: 2023-02-25
基金项目: 国家自然科学基金(61705156,60976018,61605138); 国家基金委区域联合基金(U21A20492)
Supported by National Natural Science Foundation of China(61705156,60976018,61605138); The Joint Funds of the National NSFC(U21A20492)

的可逆光色转换,非对称的**DBT**分子则表现为不可逆光色转换。本研究为基于苯并噻二唑类刺激响应发光材料提供了重要的分子设计思路。

关　键　词: 苯并噻唑; 机械响应; 多色发光

1　Introduction

Development of organic luminescent material is of great importance for their applications in organic light-emitting diodes (OLEDs), sensors, bioimaging and displays[1-3]. Multicolor emission in a single molecule, resulting from external stimuli such as solvent, aggregate state and external forces, endows organic compound unique applications, such as ink security, sensors and disease detectors[4-7]. Mechanochromic responses luminescence (MRL) mainly depends on molecular conformations and packing structures in solid state[8-9]. This kind of materials usually have donor (D) with flexible structure and acceptor (A) units, which facilitate adjustment of emission colors. In addition, the luminescent behaviors of D-A-type emitter are inclined to be affected by surrounding environment owing to their special charge transfer (CT) transition[10-11]. Consequently, their excited-state properties are also sensitive to external stimuli[12-15]. For example, asymmetrical molecule with two different chromophores reported by Chi achieved various excited state natures including room-temperature phosphorescent (RTP), thermally activated delayed fluorescence (TADF) and mechano-responsive luminescence (MRL) in a single molecule due to different dominant chromophore under excitation[16]. The D-A-type of TRZ-c-BPXZ exhibited on-off switchable crystal-dependent TADF feature[17]. Strong afterglow and dual emissive were achieved successfully by bridging dibenzofure moieties[18]. Simultaneously, these materials with abundant excited state nature and emission colors benefit to investigate the relationship between molecular packing and configuration[19-20].

2,1,3-benzothiadiazole (BT) and its derivatives are promising types of acceptor units, owing to their strong electron-withdrawing property, intense light absorption and good photochemical stability, which usually couples with a variety of electron-rich groups to form low band gap emitting materials[21-22]. BT derivatives have exhibited huge potential applications in organic photovoltaics (OPVs)[23], dye-sensitized solar cells, organic field effect transistor (OFETs)[24] and OLEDs[25]. Our previous work indicates that incorporating triphenylamine (TPA) can enhance OLED device performance[26]. DMAC unit in emitter with two methyl generally undergoes fold along C-N axis[16], endowing emitters with a great diversity of molecular conformations. Therefore, two molecules with D-A-D and D-A-D' structure were designed and synthesized, expecting to achieve emission colors changes by switching from one chromophore to another.

Recently, **TBT** with BT as an acceptor and two TPA as donor were reported, which possess a unique hybridized local and charge-transfer (HLCT)[27-28]. However, its interesting high-contrast crystal-dependent emission (**TBT-G**: λ_{PL}=570 nm, **TBT-Y**: λ_{PL}=593 nm and **TBT-R**: λ_{PL}=616 nm) and MRL behaviors have not been revealed. To study further the emission-changing mechanism and the role of TPA, **DBT** with D-A-D' structure using DMAC to replace TPA were also synthesized. The results show emission colors of **DBT** are also highly dependent on its conformations and three crystals were obtained, namely **DBT-Y**: λ_{PL}=570 nm, **DBT-O**: λ_{PL}=605 nm and **DBT-R**: λ_{PL}=642 nm. The asymmetrical structure for **DBT** exhibited selective of dominant chromophore result from the fold motions of DMAC. Yang and co-workers reported that DBD molecule using BT as acceptor and DMAC as donor with D-A-D structure was a typical TADF emitter[29]. While, **DBT** exhibits no delayed florescent. Their molecular structures are listed in Scheme 1. This research provided an important strategy to investigate the relationship between molecular configuration and photophysical properties.

2 Experiment

2.1 Materials and Synthesis

All reagents and solvents for synthesis and characterization were purchased from commercial companies and without further purification. **DBT** was prepared *via* simple Suzuki coupling reaction, as shown in Scheme S1. The chemical structures of target compounds were confirmed by ^{1}H NMR, ^{13}C NMR (Fig. S1 and S2). While the synthesis and structure characteristics for **TBT** were reported[27]. Its polymorphism-dependent and mechanochromic luminescent properties have not revealed thus far. The single crystals of **TBT-R** and **DBT-O** were grown from tetrahydrofuran (THF)/methanol. The crystals of **TBT-Y** were prepared from dichloromethane (DCM)/methanol and **DBT-R** were obtained from the DCM/methanol/ethanol.

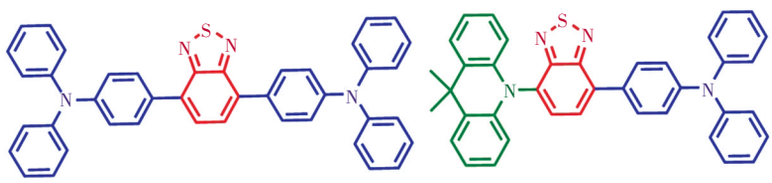

TBT **DBT**

Scheme 1 Molecular structures of **TBT** and **DBT**

2.2 Characterizations

^{1}H-NMR and ^{13}C-NMR spectra were measured with a Switzerland Bruker DR×600 at 600 MHz and 151 MHz using tetramethylsilane(TMS) as the internal standard. UV-Vis spectra were recorded using a Hitachi U-3900 spectrometer. Photoluminescence (PL) spectra were recorded with a Horiba FluoroMax-4 spectrometer. The transient photoluminescence decay was carried out using an Edinburgh Instrument FLS980 spectrometer. Thermal gravimetric analysis was performed on a Netzsch TG 209F3 under dry nitrogen atmosphere. Differential scanning calorimetry (DSC) was measured on DSC Q2000. Powder X-ray diffraction were recorded using Bruker APEX-Ⅱ CCD diffractometer with a graphite-monochromated Mo Kα radiation (Bruker Corporation, Billerica, MA, USA). Molecular structures were determined by direct methods with SHELXS-97/SHELXL-97.

The electrochemical properties were obtained *via* cyclic voltammetry (CV) measurement by using a CHI 660E voltammetry analyzer. Tetrabutylammoniumhexafluorophosphate ($TBAPF_6$) in anhydrous dichloromethane (0.1 mol/L) was used as the electrolyte. A platinum wire was used as the working electrode. A platinum electrode was the counter and a Ag/AgCl system was used as reference electrode with ferrocenium-ferrocene (Fc^+/Fc) as the internal standard. $E_{HOMO}=-4.8-e\left(E_c^{ox}-E_f^{ox}\right)V$, $E_{LUMO}=E_{HOMO}+E_g$, $E_g=\frac{1240}{\lambda}$. Theoretical simulations were performed using the Gaussian 09 package. Geometry optimization was performed by density functional theory(DFT) in B3LYP/6-31 G(d) basis sets.

3 Results and Discussions

3.1 Photophysical Properties

The UV-Vis absorption and PL spectra of **TBT** and **DBT** were measured in DCM solution (1×10^{-5} mol/L) (in Fig. 1(a)) and data were listed in Tab. 1. The intense absorption peaks at 305 nm for **TBT** and 312 nm for **DBT**, which should be attributed to the π-π* transition. While the broad low-energy absorption band at 458 nm for **TBT** and 438 nm for **DBT** could be assigned to intramolecular charge transfer(ICT) transition from electron-donating unit to BT acceptor[30]. The PL spectra of **TBT** and **DBT** in DCM solution displayed broad emission with peaks at 662 nm and 652 nm. The large Stokes shifts indicated that their emission could be origin from the charge transfer (CT) states in the single molecular state. This result also had been proven by their PL spectra in different solvents(Fig. S3). With increasing polarity from hexane to acetonitrile, the emission spectra of **TBT** and **DBT** turned to be broaden and weaken in PL intensity.

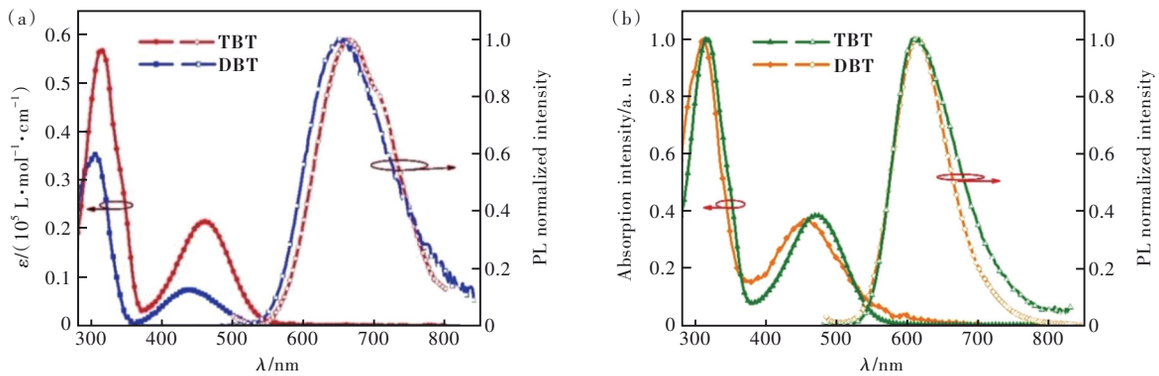

Fig.1　UV-Vis absorption and PL spectra measured in DCM solution(a) and in film(b) of **TBT** and **DBT**

Tab. 1　Photophysical data of DBT and TBT

	λ_{abs}[a]/nm	λ_{em}[b]/nm	T_d/T_g/℃	E_g[c]/eV	HOMO[d]/eV	LUMO/eV
DBT	304, 437 /315, 472	662/615	360/112	2. 26	−5. 34	−3. 08
TBT	315, 460 /312, 456	651/609	375/100	2. 28	−5. 20	−2. 92

[a] The absorption peak in DCM/film; [b] the emission peak in DCM solution/film; [c] energy gap; [d] energy of HOMO.

For the aggregate state, the PL emission peaks of **TBT** and **DBT** in the films were located at 609 nm and 615 nm with the similar profiles (Fig. 1 (b)). To verify emission behaviors of two molecules, the transient PL spectra in films were measured, as can be seen in Fig. S4. The fluorescent lifetime(τ) of **TBT** at 609 nm was 5. 71 ns. While the emission at 615 nm for **DBT** was fitted to biexponential with τ_1=3. 84 ns(27. 22%) and τ_2=8. 03 ns (72. 78%). Therefore, the emission of **TBT** and **DBT** in films originated from different excited states. As illustrated in Fig. S5, the levels of the highest occupied molecular orbitals(HOMOs) were estimated to be −5. 20 eV and −5. 34 eV for **TBT** and **DBT**. Their optical energy gaps(E_g) were calculated to be 2. 26 eV and 2. 28 eV by absorption cut-offs. Accordingly, the levels of the lowest unoccupied molecular orbitals (LUMOs) were −2. 92 eV and −3. 08 eV.

3. 2　High-contrast and Crystal-dependent Emission Behaviours

X-ray single crystal analyses were carried out to get insight into the relationship between emission and configurations, and the single-crystal data were summarized in Tab. S1. For compound **DBT**, three different crystals of **DBT-Y**(λ_{PL}= 570 nm), **DBT-O** (λ_{PL}= 605 nm) and **DBT-R** (λ_{PL}= 642 nm) were obtained by solvent evaporation method and can be divided into two groups: (1) **DBT-Y** and **DBT-R** with the folded DMAC around N-C axis; (2) **DBT-O** with a planar configuration of DMAC, as shown in Fig. 2 and Fig. 3. **DBT-Y** and **DBT-R** were monoclinic system with the space group of $P2_1/c$, presenting the rod like shapes while **DBT-O** displayed block shape.

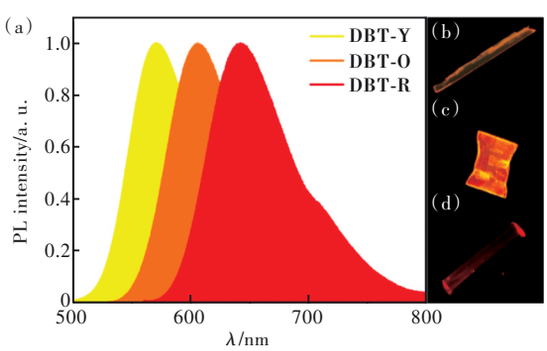

Fig.2　(a) PL spectra of **DBT** crystal. Luminescence images of **DBT-Y**(b), **DBT-O**(c) and **DBT-R**(d).

The absolute photoluminescence quantum yield (Φ_{PL}) of **DBT-Y**, **DBT-O** and **DBT-R** were measured to be 12%, 10. 6% and 6%, respectively. Luminescent properties are not only origin from the single-molecule structure, but also derived from the packing modes in aggregate state[31]. The molecular packing of **DBT-Y** and **DBT-R** were presented in Fig. S3 and Fig. 3. Their intramolecular and intermolecular interactions were listed in Tab. S3. The adjacent intermolecular π - π stacking occurred

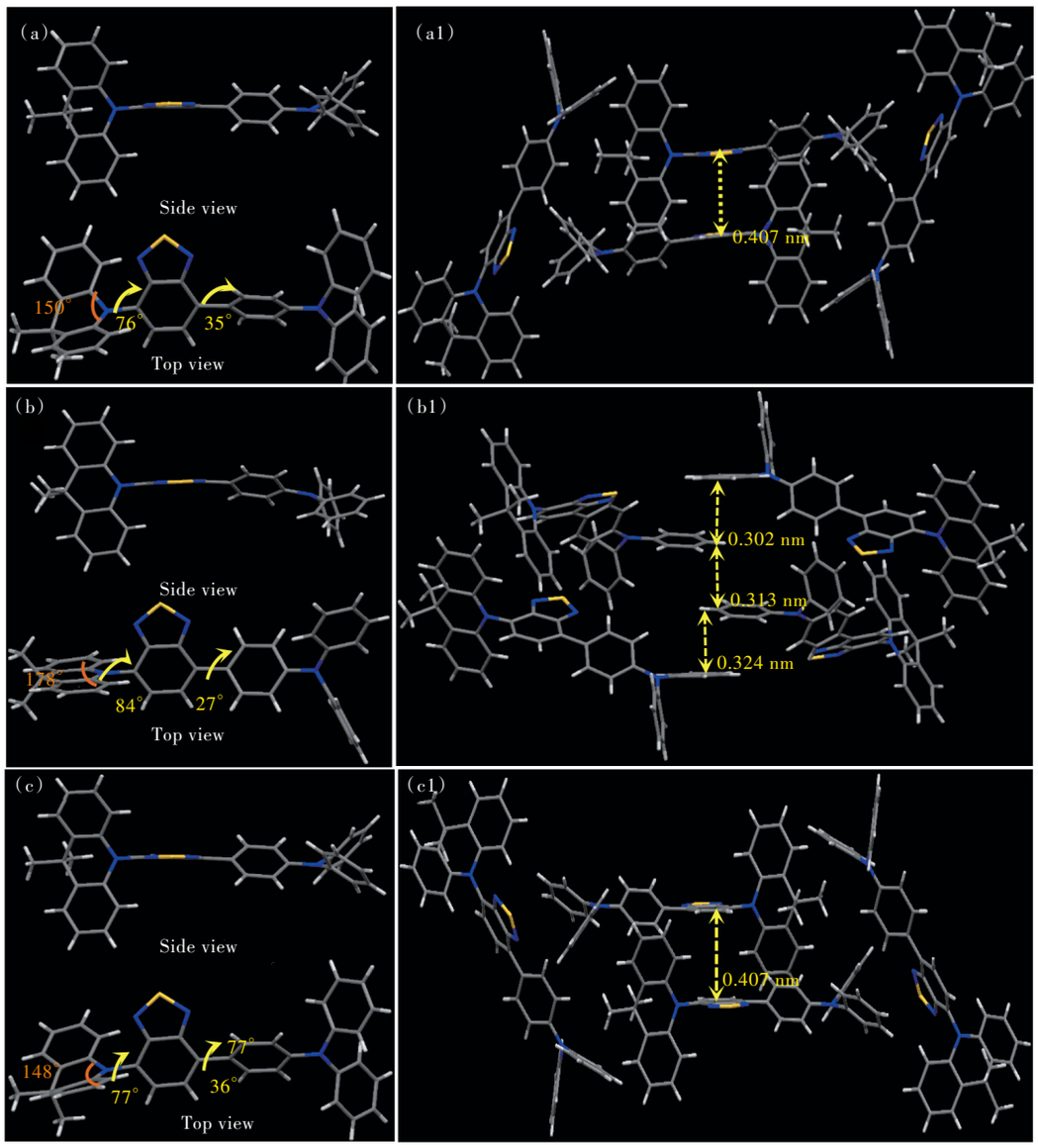

Fig.3 Single-crystal structures and molecular packing of **DBT-Y**(a, a1), **DBT-O**(b, b1) and **DBT-R**(c, c1).

between BT units through tail-to-head antiparallel arrangement with the distance larger than 0.407 nm. **DBT-R** exhibited a little shorter distances than that of the **DBT-Y**, indicating a compact packing. The folded angles of DMAC in **DBT-Y** and **DBT-R** were 150° and 148°.

These differences in molecular interactions and folded angles resulted in different photophysical properties[32]. For **DBT-O**, it exhibited the orthorhombic system with *Pbca* space group and a planar DMAC unit. The strong π-π interaction of 0.302, 0.313, 0.324 nm by parallel arrangement between benzene rings of TPA were observed in crystalline stacking. For **DBT-O** molecule, there was not only intramolecular interaction C—H···N of 0.227 9 nm, but also the intermolecular interaction C—H···N of 0.293 9 nm. The single crystal of **DBT-Y** and **DBT-O** exhibited single exponential with 10.84 ns and 6.81 ns, while the decay curve **DBT-R** fitted to biexponential with τ_1=5.77 ns (24.71%) and τ_2=4.53 ns(75.29 %), as exhibited in Fig. S7.

For compound **TBT** with the symmetrical structure, two different crystals with high-contrast emission were also prepared by solvent evaporation methods, **TBT-Y** (λ_{PL}= 593 nm) and **TBT-R** (λ_{PL}= 617 nm), as shown in Fig. 4. The monomer **TBT** have been reported with λ_{PL}= 615 nm[27]. They were all triclinic system and *P*-1 space group. **TBT-G** with

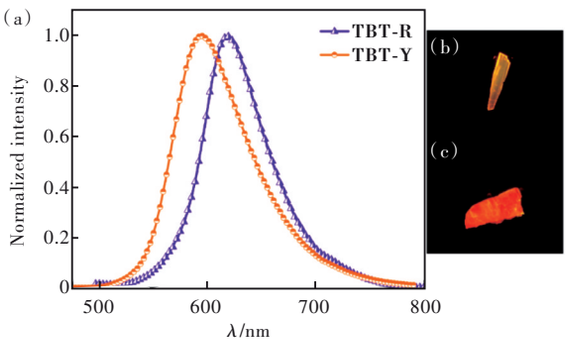

Fig.4　(a) PL spectra of TBT crystals. Luminescence images of **TBT-Y** (b) and **TBT-R** (c).

λ_{PL}= 580 nm also have been reported but no single-crystal data[22].

For **TBT-Y** and **TBT-O**, there existed four different molecules in one single crystal assembling together by close H-hydron intermolecular interaction (Fig. 5). Their torsions angle of each molecule have been listed in Fig. S8 and S9. The short contacts were listed in Tab. S4. In **TBT-Y**, two molecules were distributed in one dimension through the head-to-head pattern of BT, and the third molecule was parallel to their plane. The fourth molecule exhibits the "ax" model, while the BT unit is perpendicular to the adjacent molecules, as shown in Fig. 5(a1). In a single molecule, the intramolecular interactions of C—H…N were not the same, indicating **TBT** was not strictly symmetrical as its chemical structure. There was only intramolecular C—H…N interaction. While, for **TBT-O**, three molecules were localized at horizontal direction, and the fourth molecule seated at the vertical direction by BT group. The intramolecular and intermolecular actions in **TBT-R** were shorted than that of in **TBT-Y**, suggesting a close packing and a red shifted emission. The crystal data for **DBT** and **TBT** have been deposited in the Cambridge Crystallographic Data Centre (CCDC)

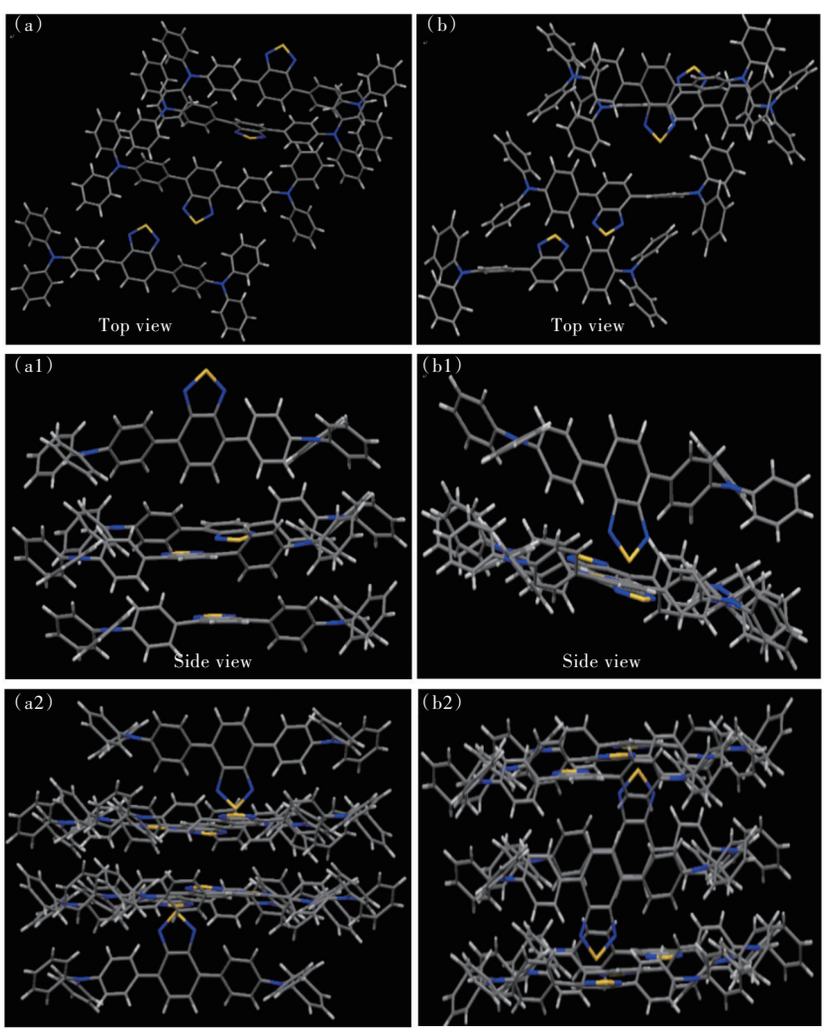

Fig.5　The single-crystal structures and packing of **TBT-Y** ((a), (a1), (a2)) and **TBT-O** ((b), (b1), (b2))

with the numbers(CCDC 2160951-2160953, 2052993, 2174557 and 2174564).

3.3 Emission Behaviors Responding to External Stimuli

It was feasible to adjust the emission colors of these crystals through external force stimuli. As shown in Fig. 6(a), the emission peak of single crystal **DBT-O** occurred the red-shift from 609 nm to 618 nm with the enhancement of emission intensity by grinding. In contrast, upon grinding, the crystal of **DBT-R** displayed a blue-shift emission from 641 nm to 621 nm with sharply increasing PL intensity (Fig. 6(b)). The single crystals of **DBT-O** and **DBT-R** have the obvious and intensity diffraction peaks, but the peaks disappeared (Fig. 7(a)) after grinding. This indicated the transform from crystal to amorphous. The opposite MRL nature of **DBT-O** and **DBT-R** may be resulted from their different molecular conformation and intermolecular interactions. **DBT-O** shows compact staking, which were difficult to destroy to form a new packing mode. While, **DBT-R** possess loosely packing, which was easily collapsed when we gave it an external stimulus and resulting a blue-shifted emission.

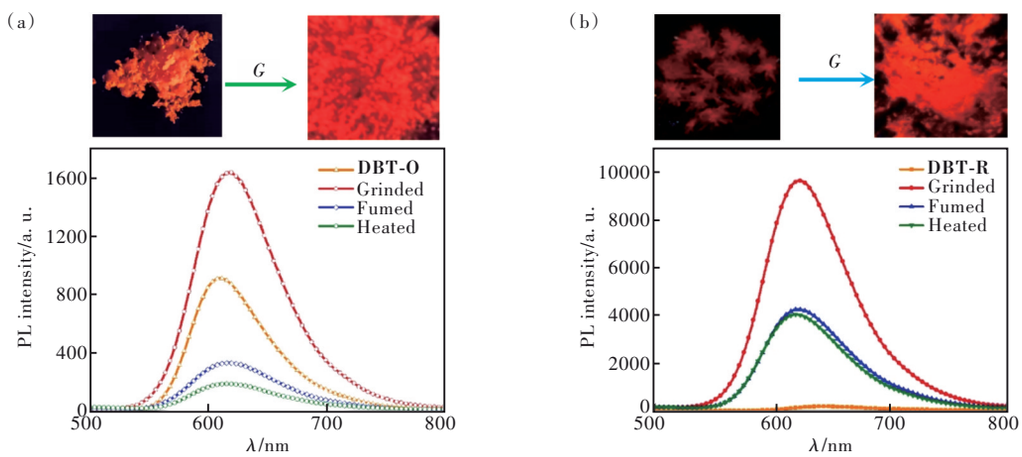

Fig.6 Fluorescent photographs under UV irradiation with 365 nm and PL spectra of **DBT-O**(a) and **DBT-R**(b) in response to external stimuli

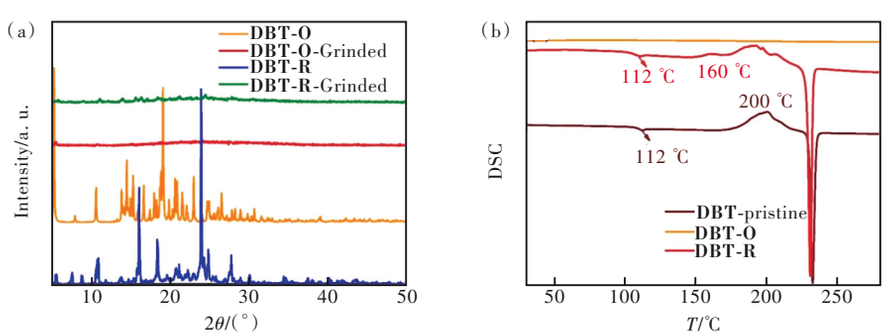

Fig.7 The XRD patterns(a) and DSC curves(b) of **DBT-O** and **DBT-R**

To further study the MRL properties of **DBT**, differential scanning calorimetry (DSC) were performed. As presented in Fig. 7(b), pristine powder and **DBT-R** show endothermic peaks at 230 ℃ and 232 ℃, which are assigned to their melting points. And there are endothermic peaks at 112 ℃, which are identical as glass transition point. **DBT-R** displayed an exothermic peak at 160 ℃, accompanied with the obvious emission peak change from 640 nm to 620 nm. Thus, this point may be ascribed to the thermal phase transition process. This result suggests that **DBT-R** was metastable phase and could be turned to a more stable state. No obvious exothermic or endothermic peaks for **DBT-O** were observed during whole heating process, which suggest that it is difficult to change the packing mode of **DBT-O**. Therefore, **DBT-O** only show 10 nm red shift in response to external stimuli no matter fuming, heating

or grinding.

For **TBT**, upon grinding pristine powder with a mortar and pestle, the emission shifted from 572 nm to 598 nm with the increasing the emission intensity (in Fig. 8(b)). XRD pattern showed that the diffraction peaks sharply reduced after grinding samples, suggesting a transform from well-order crystalline phase to amorphous. When fuming the grinded sample with DCM vapor, it turned to yellow light with the PL peak at 580 nm with some intense diffraction peaks appeared again, indicating that it is a microcrystalline. Then, grinding the fumed sample again, the emission of **TBT** red-shifted to 598 nm. When heating this grinded samples at 120 ℃ in the air, it converted back into pristine microcrystals with emission maximum of 573 nm. Thereafter, the pristine sample was heated to the melt point. The bright red light with the emission peak at 612 nm was observed. Thus, **TBT** achieves a reversible four colors transition.

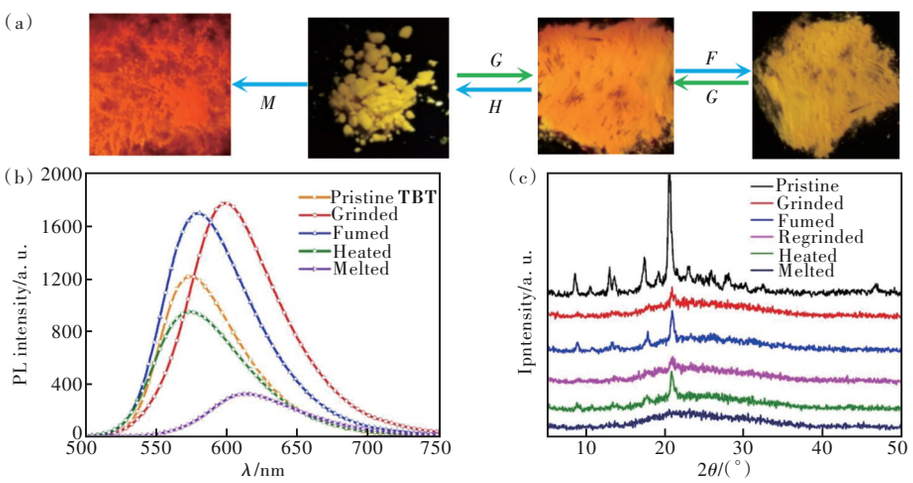

Fig.8　Fluorescent photographs(a) under UV irradiation with 365 nm, PL spectra response to external stimuli(b), XRD patterns in different states for **TBT**(c).

TBT showed four colors reversible switches in response to the external stimuli with a large span from yellow to red. Except for **DBT-Y**(A few of single crystal **DBT-Y** were obtained, it is difficult to investigate the MCL properties), **DBT-O** and **DBT-R** exhibit bicolor change with the smaller emission shift in emission peaks and their MRL emissive behaviors are irreversible.

3.4　Density Function Theory Calculations

The density functional theory calculations were performed on the two compounds to get insight about the luminescent mechanism by using the single crystal data as input file. The ground state(S_0) optimization of **TBT** and **DBT** were carried out by using the basis set B3LYP-631G(d, p) by employing crystal data as input file. The results demonstrated that, for **DBT-Y** and **DBT-R**, HOMOs were all mainly localized on the TPA moiety, which was the dominant chromophore(Fig. S10). While, HOMO of **DBT-O** was all distributed on the DMAC unit. The LUMOs of three different crystals were on the electron-withdrawing BT groups. The planar DMAC exhibits stronger donating-electron ability than TPA. The calculated HOMO/LUMO of **DBT-Y**, **DBT-O** and **DBT-R** are −5.11/−2.54 eV, −4.87/−2.46 eV and −5.12/−2.56 eV, respectively.

For **TBT**, their HOMOs distributed on the whole molecular skeleton, while the LUMOs were mainly on the BT acceptor, as shown in Fig. S10. The difference was that the HOMO and LUMO of tetramer **TBT-O** and **TBT-R** were appeared on different molecules, suggesting that the transition from HOMO to LUMO were intermolecular.

4　Conclusions

In conclusion, we have developed two crystal-dependent emitting materials of symmetrical **TBT** and asymmetric **DBT**. Compound **TBT** exhibited two kinds crystals of **TBT-O**(λ_{PL}= 593 nm) and **TBT-R**(λ_{PL}= 617 nm) with different packing structures.

DBT possessed three kinds crystals of **DBT-Y** (λ_{PL}= 570 nm), **DBT-O** (λ_{PL}= 605 nm) and **DBT-R** (λ_{PL}= 642 nm), respectively. The results showed that different emission colors resulted from the folded angles of DMAC units. Upon external stimuli, their emission colors in single crystals can be adjusted. Crystals **DBT** shows reverse bicolor change behavior, while **TBT** exhibit four reversible color-switching properties. The relationship between molecular configuration and emission were deeply explored. The emission peaks of **TBT** and **DBT** were located at 662 nm and 652 nm in DCM, 609 nm and 615 nm in films. Our work will promote the development of the multicolor emitting materials based on BT groups.

Supplementary Information and Response Letter are available for this paper at: http://cjl.lightpublishing.cn/thesisDetails#10.37188/CJL.20230022.

References:

[1] XU Y C, WANG Q Y, CAI X L, *et al*. Highly efficient electroluminescence from narrowband green circularly polarized multiple resonance thermally activated delayed fluorescence enantiomers [J]. *Adv. Mater.*, 2021, 33(21): 2100652-1-9.

[2] 李梦珂, 陈子健, 邱伟栋, 等. 纯有机电致室温磷光材料与器件研究进展 [J]. 发光学报, 2023, 44(1): 90-100.
LI M K, CHEN Z J, QIU W D, *et al*. Progress of purely organic room-temperature electrophosphorescent materials and devices [J]. *Chin. J. Lumin.*, 2023, 44(1): 90-100. (in Chinese)

[3] 张靖羚, 李凯, 杨楚罗. 过渡金属配合物TADF发光材料研究进展 [J]. 发光学报, 2023, 44(1): 12-25.
ZHANG J L, LI K, YANG C L. Advances in thermally activated delayed fluorescence of transition metal complexes [J]. *Chin. J. Lumin.*, 2023, 44(1): 12-25. (in Chinese)

[4] BARMAN D, GOGOI R, NARANG K, *et al*. Recent developments on multi-functional metal-free mechanochromic luminescence and thermally activated delayed fluorescence organic materials [J]. *Front. Chem.*, 2020, 8: 483-1-21.

[5] XIAO Z Q, LI N Q, YANG W, *et al*. Saccharin-derived multifunctional emitters featuring concurrently room temperature phosphorescence, thermally activated delayed fluorescence and aggregation-induced enhanced emission [J]. *Chem. Eng. J.*, 2021, 419: 129628-1-9.

[6] HAN X, GE F, XU J L, *et al*. Aggregation-induced emission materials for nonlinear optics [J]. *Aggregate*, 2021, 2(3): e28-1-19.

[7] LIU H C, GU Y R, DAI Y X, *et al*. Pressure-induced blue-shifted and enhanced emission: a cooperative effect between aggregation-induced emission and energy-transfer suppression [J]. *J. Am. Chem. Soc.*, 2020, 142(3): 1153-1158.

[8] SHAO B, JIN R H, LI A S, *et al*. Luminescent switching and structural transition through multiple external stimuli based on organic molecular polymorphs [J]. *J. Mater. Chem.* C, 2019, 7(11): 3263-3268.

[9] GIRISH Y R, PRASHANTHA K, BYRAPPA K, Recent advances in aggregation-induced emission of mechanochromic luminescent organic materials [J]. *Emergent Mater.*, 2021, 4(3): 673-724.

[10] OKAZAKI M, TAKEDA Y, DATA P, *et al*. Thermally activated delayed fluorescent phenothiazine-dibenzo[*a*, *j*]phenazine-phenothiazine triads exhibiting tricolor-changing mechanochromic luminescence [J]. *Chem. Sci.*, 2017, 8(4): 2677-2686.

[11] YANG W, YANG Y Y, ZHAN L S, *et al*. Polymorphism-dependent thermally activated delayed fluorescence materials with diverse three dimensional supramolecular frameworks [J]. *Chem. Eng. J.*, 2020, 390: 124626-1-9.

[12] LI H, LI H H, WANG W, *et al*. Stimuli-responsive circularly polarized organic ultralong room temperature phosphorescence [J]. *Angew. Chem. Int. Ed.*, 2020, 59(12): 4756-4762.

[13] LI B W, GONG Y B, WANG L, *et al*. Highly efficient organic room-temperature phosphorescent luminophores through tuning triplet states and spin-orbit coupling with incorporation of a secondary group [J]. *J. Phys. Chem. Lett.*, 2019, 10(22): 7141-7147.

[14] YU L, WU Z B, XIE G H, *et al*. Molecular design to regulate the photophysical properties of multifunctional TADF emitters towards high-performance TADF-based OLEDs with EQEs up to 22.4% and small efficiency roll-offs [J]. *Chem. Sci.*, 2018, 9(5): 1385-1391.

[15] PAISLEY N R, TONGE C M, MAYDER D M, *et al*. Tunable benzothiadiazole-based donor-acceptor materials for two-photon excited fluorescence [J]. *Mater. Chem. Front.*, 2020, 4(2): 555-566.

[16] LI W L, HUANG Q Y, MAO Z, *et al.* Selective expression of chromophores in a single molecule: soft organic crystals exhibiting full-colour tunability and dynamic triplet-exciton behaviours [J]. *Angew. Chem. Int. Ed.*, 2020, 59(9): 3739-3745.

[17] YANG W, YANG Y Y, CAO X S, *et al.* On-off switchable thermally activated delayed fluorescence controlled by multiple channels: understanding the mechanism behind distinctive polymorph-dependent optical properties [J]. *Chem. Eng. J.*, 2021, 415: 128909-1-7.

[18] CHEN J R, YU T, UBBA E, *et al.* Achieving dual-emissive and time-dependent evolutive organic afterglow by bridging molecules with weak intermolecular hydrogen bonding [J]. *Adv. Opt. Mater.*, 2019, 7(7): 1801593-1-7.

[19] EKBOTE A, MOBIN S M, MISRA R, Structure-property relationship in multi-stimuli responsive D-A-A′ benzothiazole functionalized isomers [J]. *J. Mater. Chem.* C, 2018, 6(40): 10888-10901.

[20] KHAN F, EKBOTE A, MOBIN S M, *et al.* Mechanochromism and aggregation-induced emission in phenanthroimidazole derivatives: role of positional change of different donors in a multichromophoric assembly [J]. *J. Org. Chem.*, 2021, 86(2): 1560-1574.

[21] HUANG J, QIAO X F, XIA Y J, *et al.* A dithienylbenzothiadiazole pure red molecular emitter with electron transport and exciton self-confinement for nondoped organic red-light-emitting diodes [J]. *Adv. Mater.*, 2008, 20(21): 4172-4175.

[22] ZHANG T F, ZHOU Z C, ZHENG Z, *et al.* "Simple" aggregation-induced emission luminogens for nondoped solution-processed organic light-emitting diodes with emission close to pure red in the standard red, green, and blue gamut [J]. *Adv. Photonics Res.*, 2021, 2(6): 2100004-1-8.

[23] ZHANG Y M, WANG Y F, SONG J, *et al.* Near-infrared emitting materials *via* harvesting triplet excitons: molecular design, properties, and application in organic light emitting diodes [J]. *Adv. Opt. Mater.*, 2018, 6(18): 1800466-1-19.

[24] BOEHME S C, YIMGA N T, FRICK A, *et al.* Correlating ultrafast dynamics, liquid crystalline phases, and ambipolar transport in fluorinated benzothiadiazole dyes [J]. *Adv. Electron. Mater.*, 2021, 7(8): 2100186-1-13.

[25] TAVAKOLI M M, PO R, BIANCHI G, *et al.* Efficient and stable mesoscopic perovskite solar cells using a dopant-free D-A copolymer hole-transporting layer [J]. *Sol. RRL*, 2021, 5(4): 2000801-1-8.

[26] ZHANG J, ZHAO Y P, XU H X, *et al.* Novel blue fluorescent emitters structured by linking triphenylamine and anthracene derivatives for organic light-emitting devices with EQE exceeding 5% [J]. *J. Mater. Chem.* C, 2019, 7(35): 10810-10817.

[27] ZHANG D, YANG T T, XU H X, *et al.* Triphenylamine/benzothiadiazole-based compounds for non-doped orange and red fluorescent OLEDs with high efficiencies and low efficiency roll-off [J]. *J. Mater. Chem.* C, 2021, 9(14): 4921-4926.

[28] JADHAV T, DHOKALE B, MOBIN S M, *et al.* Mechanochromism and aggregation induced emission in benzothiazole substituted tetraphenylethylenes: a structure function correlation [J]. *RSC Adv.*, 2015, 5(38): 29878-29884.

[29] NI F, WU Z B, ZHU Z C, *et al.* Teaching an old acceptor new tricks: rationally employing 2, 1, 3-benzothiadiazole as input to design a highly efficient red thermally activated delayed fluorescence emitter [J]. *J. Mater. Chem.* C, 2017, 5(6): 1363-1368.

[30] CHEN X J, YANG Z, LI W L, *et al.* Nondoped red fluorophores with hybridized local and charge-transfer state for high-performance fluorescent white organic light-emitting diodes [J]. *ACS Appl. Mater. Interfaces*, 2019, 11(42): 39026-39034.

[31] 李爱森, 王金凤, 李振. 分子堆积——影响固态有机小分子力响应发光行为的关键因素 [J]. 发光学报, 2021, 42(3): 283-295.
LI A S, WANG J F, LI Z. Molecular stacking-key factor in mechanical-responsive luminescent behaviors of solid organic small molecules [J] *Chin. J. Lumin.*, 2021, 42(3): 283-295. (in Chinese)

[32] ZHENG K L, NI F, CHEN Z X, *et al.* Polymorph-dependent thermally activated delayed fluorescence emitters: understanding TADF from a perspective of aggregation state [J]. *Angew. Chem. Int. Ed.*, 2020, 59(25): 9972-9976.

董书凡(1999–),男,江西景德镇人,硕士研究生,2020年于太原理工大学获得学士学位,主要从事有机发光小分子与电致发光二极管制备的研究。
E-mail: 1604067404@qq.com

许慧侠(1981–),女,河南长垣人,博士,副教授,硕士生导师,2010年于太原理工大学获得博士学位,主要从事有机光电材料与器件的研究.
E-mail: xuhuixia@tyut.edu.cn